ACS OMEGA

http://pubs.acs.org/journal/acsodf

Article

Combined Ultraviolet Ozone and Thermally Activated Formamidinium Iodide Solution to Fabricate Large Grain $FAPbI_{2.6}Br_{0.3}Cl_{0.1}$ Films

Bhabani Sankar Swain,* Son Singh, Rahim Abdur, Jae-Hun Kim, and Jaegab Lee*

Cite This: *ACS Omega* 2023, 8, 9298−9306

Read Online

ACCESS | Metrics & More | Article Recommendations | Supporting Information

ABSTRACT: In this report, we report the fabrication of a large grain and high crystallinity perovskite film by combined ultraviolet-ozone (UVO) and thermal treatment of formamidinium iodide solution during the fabrication of formamidinium lead halide ($FAPbI_{2.6}Br_{0.3}Cl_{0.1}$) films by a two-step deposition method. In this process, lead halide films were treated with UVO-treated FAI at different times. In addition, we have observed that hot-casting of UVO-assisted FAI nucleates the α-$FAPbI_3$ phase in as-prepared films. Again, we observed that the annealed hot-cast UVO-assisted FAI increased the grain size and crystallinity in the films. It was observed that the perovskite film fabricated using 10 min UVO-treated FAI solution shows the highest power conversion efficiency (PCE) up to 17.74%. Furthermore, the perovskite film fabricated with the hot-cast at 120 °C with the 10 min UVO-treated FAI solution improved the PCE to 19.22%. This finding would help with fabrication of large grain, smooth, uniform, and pinhole perovskite films by combining UVO and thermally assisted FAI solution.

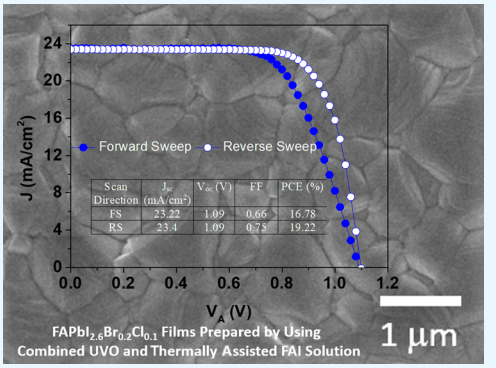

INTRODUCTION

Formamidinium lead halide ($FAPbX_3$) perovskite materials have been a better absorber material compared to methylammonium lead halide ($MAPbX_3$) in terms of stability of moisture and humidity conditions.[1,2] $FAPbX_3$ also has high thermal and electrical stability for long-term operation.[3−5] Perovskite solar cells (PSC) need to be compact, uniform, dense, defect-free, and pinhole-free with pure α-$FAPbI_3$ large grains with a minimal grain boundary which enhances the device's performance. So far, three major deposition methods were adopted to fabricate $FAPbI_3$ perovskite including a one-step process,[6] two step-process,[7] and co-thermal evaporation and vapor phase growth to fabricate $FAPbI_3$.[8−13] In the one-step deposition method, equimolar PbI_2 and FAI are dissolved in an appropriate solvent mixture and spin-cast and annealed at an appropriate temperature. In addition to that, with a little modification to one-step deposition, several efforts such as antisolvent engineering,[14] additive engineering,[15−17] and solvent and solution engineering could also help to fabricate uniform, dense, and pinhole-free perovskite films.[18,19]

Low-temperature fabrication of α-$FAPbI_3$ was reported in methylammonium thiocyanate (MASCN) or formamidinium ammonium thiocyanate (FASCN) vapor treatment of δ-$FAPbI_3$ perovskite films.[20] The most common practice so far is using anion additives such as bromine/chloride of a different element, which can modify the crystallization process and can annihilate the defect density and passivate the surface of perovskite films. So carefully choosing metal halides or methylammonium halides with an appropriate molar ratio is a pivotal role to stabilize α-$FAPbI_3$.[21−24] Similarly, alkaline metal chloride additive mixed with presynthesized $FAPbI_3$ along with an antisolvent engineering method using diethyl ether, Lyu et al. stabilized an α-$FAPbI_3$ perovskite film at 150 °C.[25,26] Similarly, a metal with a comparative same ionic radius (Bi, Ru) can be used to stabilize α-$FAPbI_3$ at low temperatures.[27] Another strategy to stabilize α-$FAPbI_3$ is to use a low ionic radius metal halide (alkali and alkaline) which can passivate the intrinsic defect density as well as stabilize the perovskite structure.[7−9] Li et al. used a strategic flash crystallization method to fabricate large grain α-$FAPbI_3$.[3] Liu et al. claimed that the δ-to-α phased transformation of $FAPbI_3$ is due to microstructure. Using presynthesized $FAPbI_3$ powder with a solution method and then in DMF/DMSO solvent in the spin-casting process, Zhang et. al achieved high efficiency (>21%).[28] Deng et al. successfully stabilized the $FA_{1-x}MA_xPbI_yBr_{3-y}$ films using methylammonium lead bromide (MABr) instead of antisolvent as post-treatment of $FAPbI_3$.[29]

Received: November 26, 2022
Accepted: February 14, 2023
Published: February 28, 2023

Especially, in the two-step deposition method, PbI_2 in DMF/DMSO and FAI was spin-coated sequentially to achieve $FAPbI_3$ film. In general, the two-step method is more desirable compared to one-step processed $FAPbI_3$ due to better control over surface morphology, defect density compactness, and pinhole-free films. To overcome the issues of low-temperature deposition, two unique methods were adopted: (a) photo-assisted FAI solution[7] and (b) thermally treated FAI solution.[30] Both methods dissociate FAI into charge ion species (FA^+ and I^-), which facilitate the nucleation of $FAPbI_3$.[7,30] In particular, the I^- ions provide extra iodine which reduces the defect density of $FAPbI_3$ films.[7,30] Lee et al. reported large grain $FAPbI_3$ crystals fabricated by a sequential deposition method using PbI_2 and photoassisted FAI solution. Their results show an optimum dose of 1 Sun exposure for 60 min which dissociates FAI into FA^+ and I^-, which can make a defect-free $FAPbI_3$ crystal.[7] It has already been experimentally proved that dissociation of both MAI and FAI took place just by keeping the solution for several hours. FAI and MA, both can be dissociated into their charge ion species by thermal treatment. The insufficient way to fabricate pure $FAPbI_3$ by the two-step deposition (TSD) is mainly because of the ionic radius of FA^+ and I^-. By just visually comparing the evolution of color of $MAPbI_3$ and $FAPbI_3$ films, it has been observed that $MAPbI_3$ turned to black color as soon as MAI dropped onto PbI_2. However, $FAPbI_3$ does not behave in the same way as $MAPbI_3$. $FAPbI_3$ needs annealing to at least 150 °C to stabilize α-$FAPbI_3$. It should be noted here that the room temperature phase of $FAPbI_3$ is the δ-phase which is a yellow phase. The δ-$FAPbI_3$ phase has a band gap of 2.42 eV, and the LUMO and HOMO levels are comparatively more than those of α-FAPbI3 which is not suitable for light harvesting.[31]

Inspired by the above research, we believe a UVO-treated FAI solution would provide a fast and efficient way to dissociate FAI solution into FA^+ and I^-, which provides free I^- ions and can be an alternative way to fabricate pure α-$FAPbI_{2.6}Br_{0.3}Cl_{0.1}$ perovskite films. In this article, we report a rapid and time-saving processing of α-$FAPbI_{2.6}Br_{0.3}Cl_{0.1}$ perovskite film by a combined UVO and thermal activation process. Herein, we demonstrate the effect of UVO treatment of FAI solution on the evolution of $FAPbI_3$ phases and the corresponding optical properties of α-$FAPbI_{2.6}Br_{0.3}Cl_{0.1}$ perovskite. We observed that an optimum 5 min UVO treatment is sufficient to dissociate FAI into FA^+ and I^- ions, which can reduce the defect density of $FAPbI_3$ films. We also observed that hot FAI casting can effectively form in α-$FAPbI_{2.6}Br_{0.3}Cl_{0.1}$ phase as-synthesized films, which eventually completely transform to the α-$FAPbI_{2.6}Br_{0.3}Cl_{0.1}$ phase after annealing at 150 °C. We fabricated a planar heterojunction α-$FAPbI_{2.6}Br_{0.3}Cl_{0.1}$ perovskite solar cell with SnO_2 and TiO_2 as the electron transport layer (ETL) and Spiro-OMeTAD as the hole transport layer (HTL) and achieved a power conversion efficiency of 19.22%.

EXPERIMENTAL SECTION

Fabrication of Perovskite Films. We used Corning glass for the deposition and characterization of the $FAPbI_{2.6}Br_{0.3}Cl_{0.1}$ perovskite film. The Corning glass was cleaned with acetone, ethanol, and deionized (DI) water, each for 30 min followed by nitrogen blowing. Before deposition, the glass substrates were exposed to ultraviolet ozone (UVO) for 30 min to make the substrate hydrophilic. We chose $PbI_{2.6}Br_{0.3}Cl_{0.1}$ (PbI_2 = 0.8M, $PbBr_2$ = 0.3M, and $PbCl_2$ = 0.1M) as the lead halide source in mixed solvents of dimethylformamide (DMF):dimethyl sulfoxide (DMSO) = 4:1 (volume ratio). The solution was stirred at 70 °C for 12 h. Lead halide film was spin-coated at 3000 rpm for 30 s and annealed at 100 °C for 5 min. FAI was dissolved in anhydrous 2-propanol and stirred for 30 min to ensure FAI was completely dissolved. The FAI solution was then UVO-treated at different times which were used in the second stage of spin-coating. The films were annealed at 150 °C at different times to study the effect of annealing time.

Fabrication of Perovskite Solar Cells. Fluorine doped tin oxide (FTO)/glass (Sigma-Aldrich, Korea) of resistivity 7 Ω/□ was cut into 2 cm × 2 cm and etched by Zn nanopowder and 50% hydrochloric acid (HCl) solution. The FTO/glass substrates were cleaned sequentially using a standard cleaning procedure, and the perovskite film was deposited by the above method. We used mesoporous anatase titania (m-TiO_2) and tin oxide (SnO_2) as electron transport layers. For TiO_2 films, a compact layer of TiO_2 was deposited using 0.3 mM titanium disopropoxide (Sigma-Aldrich, Korea) in 1-butanol at 3000 rpm for 30 s. To make the film compact, it was preannealed at 120 °C for 10 min and then annealed at 500 °C for 1 h in an ambient air atmosphere. m-TiO_2 was prepared in diluted ethanol in which the v/v ratio of m-TiO_2 to ethanol was 3.5:1. Before deposition of the perovskite layer, the films were treated with UVO for 30 min. For SnO_2 film deposition, 2.5 wt % SnO_2 (Alpha-Caesar, Korea) nanoparticles were spin-coated at 3000 rpm for 30 s. The annealing time of the SnO_2 film was 150 °C for 30 min.

The FAI solution was prepared by two different processes: (a) UVO-assisted and (b) thermally assisted. For the UVO assisted process, the FAI solution was placed under UVO (282 and 365 nm) at different times (1−30 min). For the thermally activated process, the FAI solution was stirred under 120 °C at different times. The resulting FAI solutions prepared by the above process were used as FAI solutions to fabricate the perovskite films. The films were annealed on a preheated hot plate at different temperatures and different times to optimize the process. After that, Spiro-OMeTAD was spin-coated at 4000 rpm for 30 s. To prepare the Spiro-OMeTAD solution, Spiro-OMeTAD (72 mg) in 1 mL of chlorobenzene and bis(trifluoromethylsulfonyl)imide lithium salt (520 mg) in 1 mL of acetonitrile were prepared separately, allowed to stir for 30 min. Then 17.5 μL of 4-*tert*-butylpyridine was added to the Spiro-OMeTAD solution and continuously stirred for another 30 min. After that, 28.8 μL of Li-salt was added and allowed to stir for another 12 h to properly mix the solvent. Finally, a 100 nm Au layer was deposited by thermal evaporation at a deposition rate of 5 Å/s.

Characterization. The microstructure of perovskite films was examined via field emission scanning electron microscopy (FESEM, JEOL JSM-6500F) operating at 5 kV accelerating voltage to analyze the surface morphologies. Energy-dispersive X-ray spectroscopy (EDX, Inca, Oxford) in addition to FESEM was used for elemental analysis of the prepared samples. The phase of the perovskite films was analyzed by X-ray powder diffraction (XRD) (Rigaku, USA, Cu $K\alpha_1$ radiation (λ = 0.1505 nm)) in 2θ mode. The absorption spectra were obtained with an ultraviolet−visible (UV−vis) spectrometer (PerkinElmer) in the visible region (400−800 nm). The current−voltage (I−V) characteristics were measured in the dark and under illumination at AM1.5G (100 mW/cm^2) with a xenon lamp (Newport, USA) connected with Keithley 2400 electrometer. The device's active area was 0.09 cm^2. The J−V

https://doi.org/10.1021/acsomega.2c07574
ACS Omega 2023, 8, 9298−9306

characteristics were measured with a voltage step 0.02 V from −0.02 to 1.2 V.

RESULTS AND DISCUSSION

Figure 1a shows the schematic diagram of the fabrication of the perovskite film by the TSD process using modified FAI solution by either thermal or UVO treatment. Figure 1b and c shows the photograph of the 0.4 M FAI solution in IPA after being treated thermally at 120 °C and UVO treatment for a different time, respectively. The color changes of the FAI solution from transparent to light yellow confirm the dissociation of FAI solution into FA^+ and I^- ions after either being treated thermally at 120 °C or with UVO treatment. It should be noted here that the color of the UVO-treated FAI solution after 30 min has a deeper color than that of the FAI solution prepared by thermal treatment at 120 °C for 960 min. Figure 1d shows the UV−vis absorption spectra of the UVO-treated FAI solution at different times. It is observed that the peak in UV−vis spectra at 355 nm which is mostly attributed to I^- ion increases with increasing UVO treatment time. This proves the dissociation of FAI solution into FA^+ and I^- after UVO treatment.

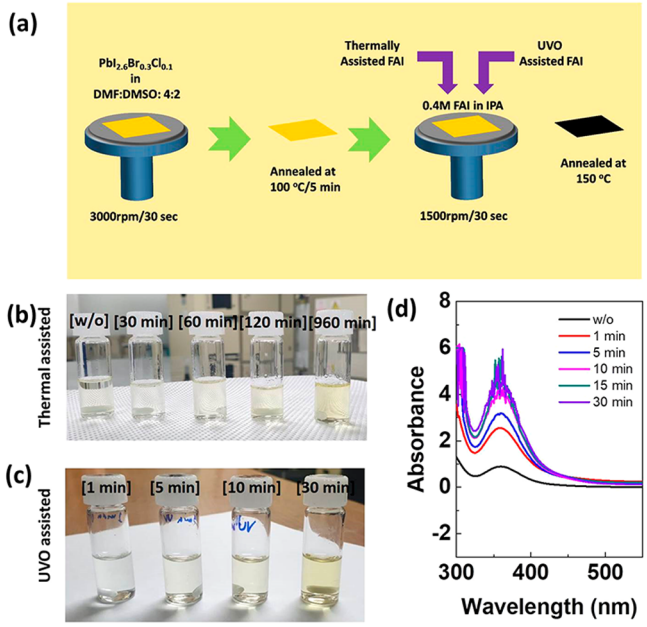

Figure 1. (a) Schematic of fabrication of perovskite films, (b) photograph of thermally assisted FAI solution, (c) photograph of UVO assisted FAI solution, and (d) UV−vis spectra of UVO-treated FAI solution for different times.

Figure 2 shows the microstructure of the perovskite film prepared by the TSD process using different UVO-treated FAI solutions for different times and annealing at 150 °C for 30 min. The untreated FAI solution-prepared perovskite film shows some pinholes and a rough surface. However, the perovskite films fabricated using UVO-treated FAI solution show a pinhole-free, compact, and smooth surface irrespective of UVO treatment time. Figure 3 shows the microstructure of perovskite film prepared by TSD using thermally treated FAI solution at 120 °C for different times and annealed at 150 °C for 30 min. In both cases, as discussed above, the average grain size increased with increasing UVO as well as thermally treated FAI solution with time, which proved to be an advantage for

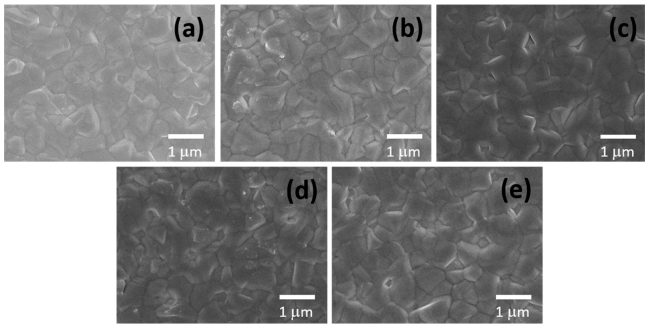

Figure 2. Microstructure of $FAPbI_{2.6}Br_{0.3}Cl_{0.1}$ films fabricated by TSD using UVO-treated FAI solution for different times: (a) without UVO, (b) 1 min, (c) 5 min, (d) 10 min, and (e) 30 min.

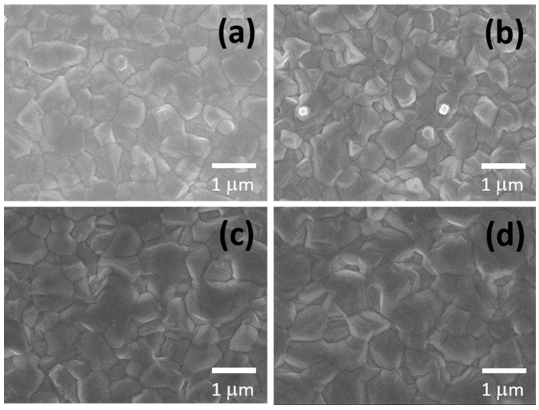

Figure 3. Microstructure of $FAPbI_{2.6}Br_{0.3}Cl_{0.1}$ films fabricated by TSD using thermally activated FAI solution at 120 °C for different times: (a) 30 min, (b) 60 min, (c) 120 min, and (d) 960 min.

the formation of perovskite films. Compact, dense, and pinhole-free perovskite films were observed with the UVO-treated FAI solution. Additionally, morphological defects such as pinholes, cracks, and regional voids have not been observed in the films. However, few shallow holes between large grains in the perovskite films were observed. Although the regional voids in the thin film are undesired, shallow holes may cause easier contact and diffusion of organic cations (MAI or FAI) in PbI_2 at the second step of the two-step solution process.

Finally, we further studied the effect of the hot casting of the UVO-treated FAI solution at different temperatures. In this experiment, the UVO-treated FAI solution for 10 min was rigorously stirred on the hot plate at different temperatures (80−140 °C). Figure 4 shows the microstructure of $FAPbI_{2.6}Br_{0.3}Cl_{0.1}$ films fabricated using hot-casting of the UVO-treated FAI solution on $PbI_{2.6}Br_{0.3}Cl_{0.1}$ films and annealed at 150 °C for 30 min. For comparison, we present the microstructure of $FAPbI_{2.6}Br_{0.3}Cl_{0.1}$ films before and after annealing at 150 °C for 30 min. Comparing the microstructure of $FAPbI_{2.6}Br_{0.3}Cl_{0.1}$ films of hot-casted UVO-treated FAI solution, it is evident that no significant changes in the microstructure were observed before and after annealing except for the smoothness of the films.

To support the microstructure presented in Figures 2−4, we analyzed the surface roughness of $FAPbI_{2.6}Br_{0.3}Cl_{0.1}$ films prepared by UVO-assisted and hot-casted UVO-assisted FAI/IPA solution. We presented the surface topography and root means square (RMS) of $FAPbI_{2.6}Br_{0.3}Cl_{0.1}$ films prepared by different process conditions. Figure 5 shows the AFM images

https://doi.org/10.1021/acsomega.2c07574
ACS Omega 2023, 8, 9298−9306

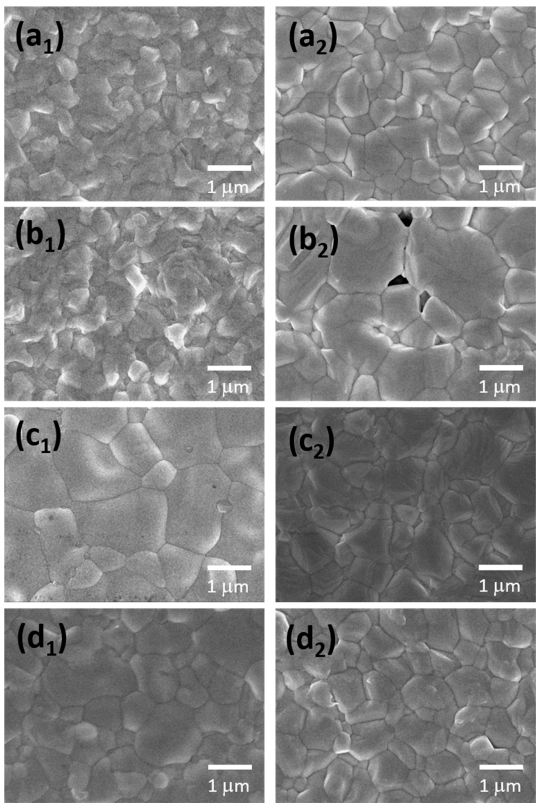

Figure 4. Microstructure of hot-casted $FAPbI_{1.6}Br_{0.3}Cl_{0.1}$ film using UVO (30 min) treated FAI/IPA hot solution at different temperatures: (a) 80 °C, (b) 100 °C, (c) 120 °C, and (d) 140 °C. Subscripts 1 and 2 represent without annealing and with annealing at 150 °C for 30 min.

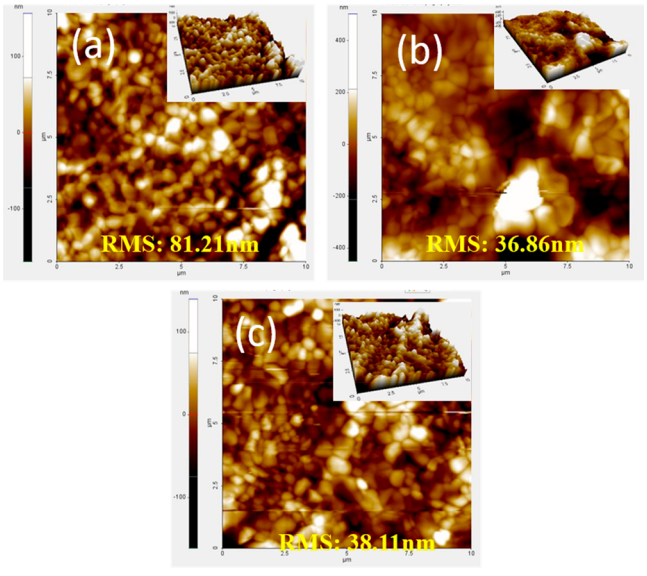

Figure 5. AFM image of perovskite films prepared using (a) pure FAI, (b) 10 min UVO-treated FAI, and (c) hot-cast at 120 °C of 10 min UVO-treated FAI solution.

of the surface topography of the $FAPbI_{2.6}Br_{0.3}Cl_{0.1}$ films: (a) as-prepared $FAPbI_{2.6}Br_{0.3}Cl_{0.1}$ (Figure 2a), (b) $FAPbI_{2.6}Br_{0.3}Cl_{0.1}$ film prepared by using 10 min UVO-treated FAI/IPA solution (Figure 2c), and (c) $FAPbI_{2.6}Br_{0.3}Cl_{0.1}$ film prepared by using hot-cast at 120 °C of 10 min UVO-treated FAI/IPA solution (Figure 4c$_2$) and the respective RMS values of above $FAPbI_{2.6}Br_{0.3}Cl_{0.1}$ films recorded as 81.21, 36.86, and 38.11 nm. The AFM images confirm that the $FAPbI_{2.6}Br_{0.3}Cl_{0.1}$ film prepared by using the UVO-treated FAI solution has better surface roughness compared to the $FAPbI_{2.6}Br_{0.3}Cl_{0.1}$ film prepared using untreated FAI/IPA solution. It is also observed that the hot-casting of UVO-treated FAI solution again increases the surface roughness of $FAPbI_{2.6}Br_{0.3}Cl_{0.1}$ film.

We studied the phase evolution of perovskite films fabricated by using UVO-treated FAI solution at different times. Figure 6a shows the XRD patterns of the $FAPbI_{2.6}Br_{0.3}Cl_{0.1}$ films

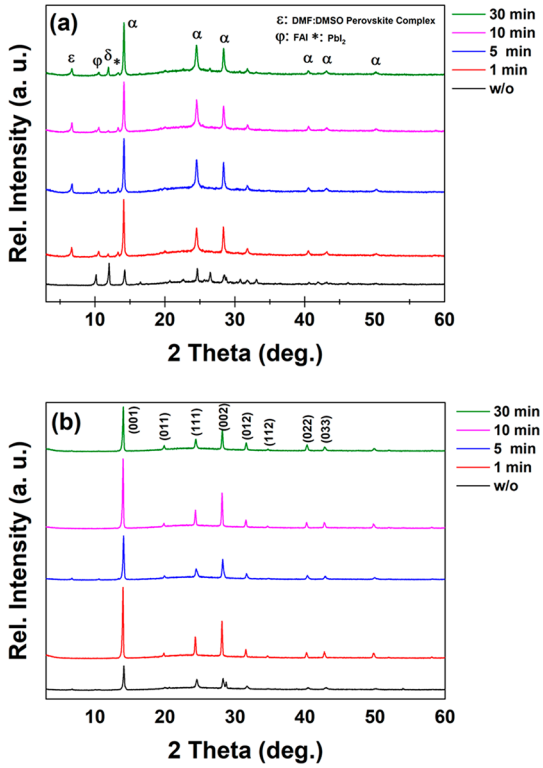

Figure 6. XRD patterns of $FAPbI_{2.6}Br_{0.3}Cl_{0.1}$ films fabricated by TSD using UVO-treated FAI solution for different times: (a) before annealing and (b) after annealing at 150 °C for 30 min.

fabricated using mixed lead halide ($PbI_{2.6}Br_{0.3}Cl_{0.1}$) and UVO-treated FAI solution for different times (1, 5, 10, 15, and 30 min) without annealing. The $FAPbI_{2.6}Br_{0.3}Cl_{0.1}$ film fabricated using FA solution without any treatment shows several peaks which include the residual PbI_2 phase, δ-phase, and α-phase of perovskite materials. The peak position appeared at 11.8° corresponding to the (010) plane of the δ-$FAPbI_{2.6}Br_{0.3}Cl_{0.1}$ phase.[1] For the as-prepared $FAPbI_{2.6}Br_{0.3}Cl_{0.1}$ film prepared using UVO-treated FAI for different times (1, 5, 10, and 30 min), the δ-phase significantly decreased when the FAI solution was UVO-treated. The peak position was at 13.9, 19.8, 24.3, 28.1, 31.4, 34.6, 40.1, and 42.7 corresponding to (001), (011), (111), (002), (012), (112), (022), and (033) of the α-$FAPbI_{2.6}Br_{0.3}Cl_{0.1}$ phase, respectively.[1] UVO-treated FAI spontaneously nucleates the α-$FAPbI_{2.6}Br_{0.3}Cl_{0.1}$ phase in the films. A similar structural transformation from the δ-phase (yellow) to the pure α-phase (black) was previously reported when the perovskite films were treated with MASCN vapor.[20] Our results demonstrated that the δ-phase was effectively suppressed in the as-prepared $FAPbI_{2.6}Br_{0.3}Cl_{0.1}$ films fab-

https://doi.org/10.1021/acsomega.2c07574
ACS Omega 2023, 8, 9298−9306

ricated by using the UVO-treated FAI solution. At the same time, the α-phase strongly appeared in perovskite film which was fabricated with the UVO-treated FAI solution. Figure 6b shows the XRD patterns of $FAPbI_{2.6}Br_{0.3}Cl_{0.1}$ films fabricated using the UVO-treated FAI solution after annealing at 150 °C for 30 min. After annealing, we observed only the α-$FAPbI_{2.6}Br_{0.3}Cl_{0.1}$ phase in the films. The δ-phase disappeared after annealing in all samples irrespective of UVO exposure time. However, the δ-phase still exists in the perovskite film which was fabricated without UVO treatment. So, it can be concluded that UVO treatment of the FAI solution has the advantage to fabricate pure α-phase $FAPbI_{2.6}Br_{0.3}Cl_{0.1}$. The increase in peak intensity, which means decreases in full width at half-maxima of the α-$FAPbI_{2.6}Br_{0.3}Cl_{0.1}$ phase, shows an improvement in crystallinity in the films.

Figure 7a shows the XRD patterns of the $FAPbI_{2.6}Br_{0.3}Cl_{0.1}$ films fabricated using mixed lead halide ($PbI_{2.6}Br_{0.3}Cl_{0.1}$) and

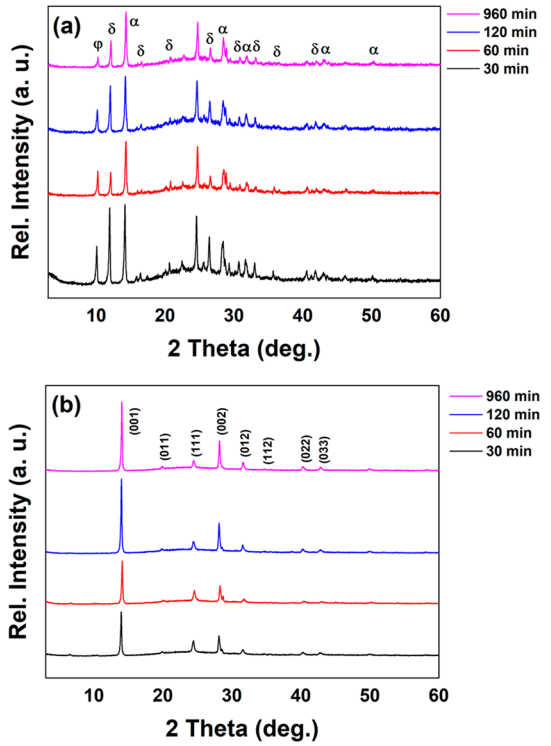

Figure 7. XRD patterns of $FAPbI_{2.6}Br_{0.3}Cl_{0.1}$ films fabricated by TSD using thermally activated FAI solution for different times: (a) before annealing and (b) after annealing at 150 °C for 30 min.

thermally activated FAI solution for different times without annealing. Unlike the perovskite films fabricated by pure FAI solution, the XRD peaks were matched with the perovskite films fabricated without using any treatment. The as-prepared $FAPbI_{2.6}Br_{0.3}Cl_{0.1}$ films without UVO treatment show two perovskite phases, δ- and α-phase with residual PbI_2 phase. However, the XRD pattern of annealed $FAPbI_{2.6}Br_{0.3}Cl_{0.1}$ film fabricated using thermally activated FAI solution shows a pure α-$FAPbI_{2.6}Br_{0.3}Cl_{0.1}$ phase. This proves that the thermally activated FAI solution stabilizes the α-$FAPbI_{2.6}Br_{0.3}Cl_{0.1}$ phase in the films. The δ-phase in the film decreased with increasing UVO treatment time. Conversely, the α-phase was increased with increasing UVO exposure time of FAI solutions. Analyzing the magnified XRD patterns of both δ- and α-$FAPbI_{2.6}Br_{0.3}Cl_{0.1}$ films, it is evident that the δ- to α-phase transformation takes place with increasing thermally activated FAI solution for 30 min. Above 30 min, both δ- and α-$FAPbI_{2.6}Br_{0.3}Cl_{0.1}$ films were decreased. These δ-phases that appeared in the perovskite films completely disappeared after being annealed at 150 °C for 30 min (Figure 7b). Interestingly, the peak intensity of α-$FAPbI_{2.6}Br_{0.3}Cl_{0.1}$ increased with increasing thermally treatment time. The peak position and full width at half-maximum (fwhm) of each peak are tabulated in the Supporting Information file (Tables S1−S3).

Again, we compared the phase evolution of perovskite film fabricated using hot-casting of UVO-activated FAI solution on $PbI_{2.6}Br_{0.3}Cl_{0.1}$ films before and after annealing. Figure 8a

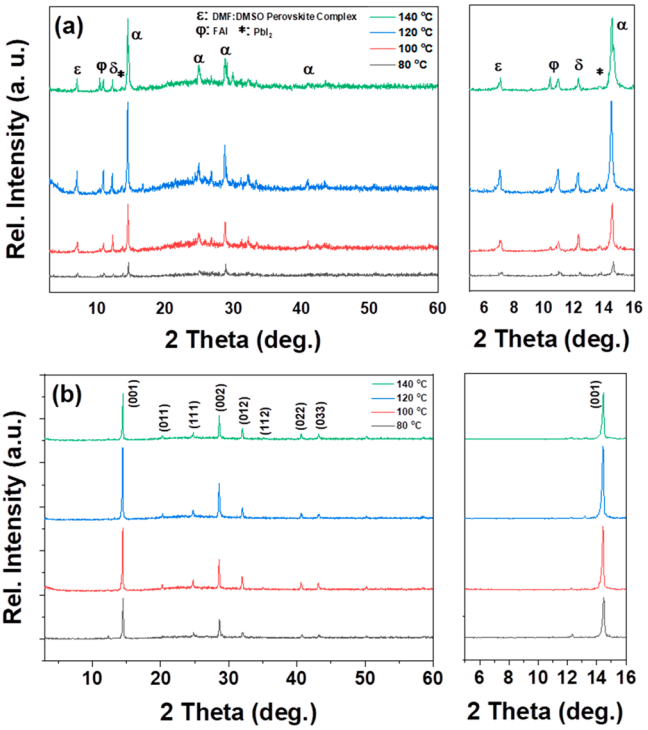

Figure 8. XRD patterns of hot-casted $FAPbI_{1.6}Br_{0.3}Cl_{0.1}$ film using UVO (30 min) treated FAI/IPA hot solution at different temperatures: (a) without annealing (as-prepared) and (b) annealing at 150 °C for 30 min.

shows the XRD patterns of $FAPbI_{2.6}Br_{0.3}Cl_{0.1}$ perovskite films using hot-casting of 5 min of UVO-activated FAI solution (without annealing). The results show that the δ-phase in the films decreased significantly with solution temperature compared to the film fabricated without hot-casting (Figure 4a). At the same time, the α-phase increased with the increase in solution temperature. The δ-phase in the $FAPbI_{2.6}Br_{0.3}Cl_{0.1}$ films completely disappeared after annealing at 150 °C for 30 min (Figure 8b). Hence, hot FAI solution casting on $PbI_{2.6}Br_{0.3}Cl_{0.1}$ films proves to be beneficial for stabilizing the α-phase in the $FAPbI_{2.6}Br_{0.3}Cl_{0.1}$ films.

The optical absorption studies of materials provide ideas about the different phases and compositions of material by analyzing the band energy edge at a different wavelength. To understand the effect of combined UVO- and thermally activated FAI solution on the formation of $FAPbI_{2.6}Br_{0.3}Cl_{0.1}$ films, we analyzed the $FAPbI_{2.6}Br_{0.3}Cl_{0.1}$ films by UV−vis absorption spectra in the range from 400 to 800 nm. Normally, the absorption band cutoff of $FAPbI_{2.6}Br_{0.3}Cl_{0.1}$ perovskite is found above 800 nm. As we doped Br and Cl in our lead halide

https://doi.org/10.1021/acsomega.2c07574
ACS Omega 2023, 8, 9298−9306

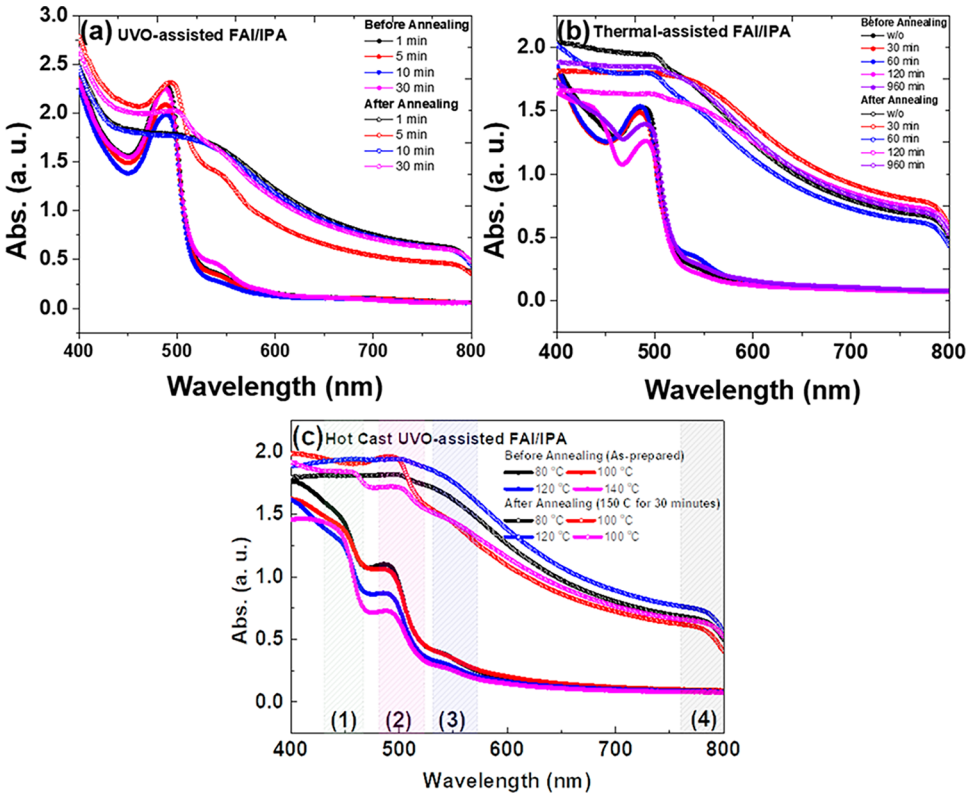

Figure 9. UV−vis spectra of $FAPbI_{2.6}Br_{0.3}Cl_{0.1}$ films fabricated by TSD using (a) UVO-treated FAI solution for different times, (b) thermally activated FAI solution for different times, and (c) hot-casted UVO assisted FAI solution at different temperature.

solution, the band energy cutoff was expected similar to the MA-based perovskite. It should be noted here that Br doping has a significantly blue-shifting band cutoff compared to Cl doping. To understand the different phases, present in the perovskite films by UVO-treated FAI solution for different times and thermally activated FAI solution at 120 °C for different times, we highlighted different regions by different colors attributed to different phases and compositions of perovskite present in our films. Figure 9a shows the comparison of UV−vis absorption spectra of perovskite films prepared by TSD using the UVO-treated FAI solution at different times before and after annealing at 150 °C for 30 min. Figure 9b shows the UV−vis absorption spectra of perovskite films prepared by TSD using thermally assisted FAI solution at 120 °C at different times. Figure 9c shows the absorption spectra of perovskite films fabricated by using hot-casted UVO-treated FAI solution at different temperatures. For comparison of absorption spectra, we present UV−vis spectra of $FAPbI_{2.6}Br_{0.3}Cl_{0.1}$ films prepared by pure, UVO-treated, and hot-casted UVO-treated FAI solution in Figure S1. As we know, the band gap of the δ-phase (yellow) and α-phase (black) perovskite film is 3.20 and 1.50 eV, respectively.[31] So, it can easily identify different phases from the absorption spectra in the spectra region 400−500 nm (green) and 750−850 nm (black color) for δ-phase and α-phase perovskite film, respectively. Residual lead halide in the perovskite film can be identified from the spectra region of 400−450 nm. From the above discussion, it can be concluded from Figure 6a that the optimum dose of 10 min of UVO to FAI solution would fabricate pure α-phase perovskite films with compact, smooth, and pinhole free perovskite film. It is observed that the δ-phase decreases with the increase in UVO treatment time of the FAI solution. This could be due to the breaking of FAI into FA^+ and I^-, for which I^- is responsible for fulfilling the I^- vacancy in the perovskite films.

From the above results, it is evident that UVO irradiation before solution-processed deposition proved to be beneficial to obtain highly uniform and smooth film deposition. The reason for the use of UVO before film deposition is to improve the surface properties by turning it into a hydrophilic surface, removing surface impurities by inducing oxygen in ambient air. So far, mostly UVO was used to improve the surface properties of the bottom transparent electrode and heal defects and impurities on the surface of the metal oxide electron transport layer in a conventional architecture as well as in the hole transport layer in the inverted architecture. Post fabrication of UV exposure leads to the degradation of PSC due to the dissociation of $MAPbI_3 = PbI_2 + MA^+ + I^-$ and also the degradation of the polymer hole transport layer (Spiro-OMeTAD. P3HT, PTAA, etc.). The dissociation of MAX and FAX into charged ion species (MA^+, FA^+, and X^-) has higher diffusivity in the perovskite crystal and may have higher diffusivity at the elevated annealing temperature. Hot-casting (FAI solution at elevated temperature) enables faster diffusion of FA^+ and I^- into the $PbI_{2.6}Br_{0.3}Cl_{0.1}$ lattice. In addition, we expect also higher diffusion of FA^+ and I^- with increasing FAI solution temperatures. Comparing the XRD data of cold and hot-casting of as-prepared UVO-assisted FAI solution shows the α-$FAPbI_{2.6}Br_{0.3}Cl_{0.1}$ phase has already nucleated in the films. It is also expected that the conversion of α-$FAPbI_{2.6}Br_{0.3}Cl_{0.1}$ is greater with the hot-casting of FAI solution onto $PbI_{2.6}Br_{0.3}Cl_{0.1}$.

We fabricated planar heterojunction PSC using combined UVO and thermally assisted FAI solution. Figure 10a shows

https://doi.org/10.1021/acsomega.2c07574
ACS Omega 2023, 8, 9298−9306

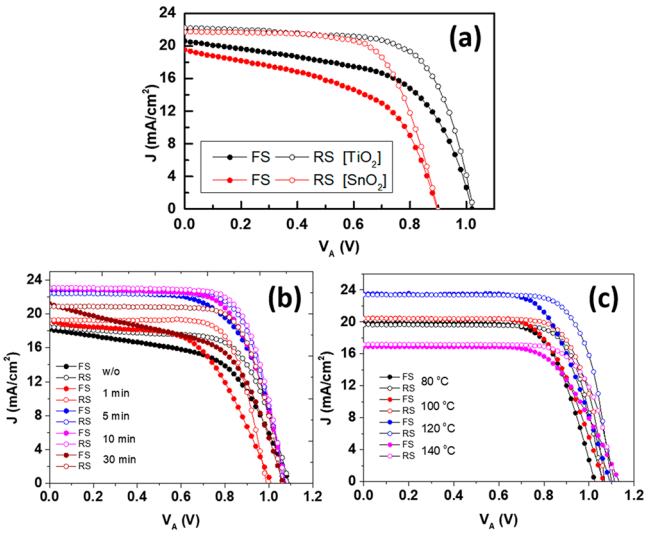

Figure 10. (a) $J-V$ curves of PSC with $FAPbI_{2.6}Br_{0.3}Cl_{0.1}$ films fabricated by using different ETL: TiO_2 and SnO_2. (b) $J-V$ curves of PSC with $FAPbI_{2.6}Br_{0.3}Cl_{0.1}$ films fabricated by TSD using UVO-treated FAI solution for different times. (c) Device parameters of $FAPbI_{2.6}Br_{0.3}Cl_{0.1}$ films fabricated by TSD using hot-cast UVO-treated FAI solutions.

the $J-V$ curve of PSC with a simple device composed of FTO/ETL/$FAPbI_{2.6}Br_{0.3}Cl_{0.1}$/HTL/Au in which 5 min UVO-treated FAI solution was used to fabricate perovskite films. We used SnO_2 and TiO_2 as the ETL and Spiro-OMeTAD as the HTL. The PV parameters such as open-circuit voltage (V_{oc}), short-circuit current density (J_{sc}), fill factor (FF), and power conversion efficiency (PCE) are summarized in Table 1. The

Table 1. Device Parameters of $FAPbI_{2.6}Br_{0.3}Cl_{0.1}$ Films Fabricated by TSD Using UVO-Treated FAI with Different ETL

ETL	scan direction	J_{sc} (mA/cm^2)	V_{oc} (V)	FF	PCE (%)
TiO_2	FS	19.51	0.9	0.52	9.10
	RS	21.69	0.9	0.67	13.12
SnO_2	FS	20.59	1.02	0.57	11.95
	RS	22.20	1.02	0.68	15.50

best-performing device shows a PCE of 9.1% (V_{oc} = 0.9 V, J_{sc} = 19.51 mA/cm^2, and FF = 0.52) and 11.95% (V_{oc} = 1.02 V, J_{sc} = 20.59 mA/cm^2, and FF = 0.57) for TiO_2 and SnO_2 ETL in forward sweep condition, respectively. The best-performing device shows a PCE of 13.12% (V_{oc} = 0.9 V, J_{sc} = 21.69 mA/cm^2, and FF = 0.67) and 15.50% (V_{oc} = 1.02 V, J_{sc} = 22.2 mA/cm^2, and FF = 0.68) for TiO_2 and SnO_2 ETL in reverse sweep condition, respectively. PSC with SnO_2 ETL shows a significantly higher efficiency compared to the PSC with TiO_2 ETL due to comparatively a higher current density and open circuit voltage. The $J-V$ characteristics of the PSC using the $FAPbI_{2.6}Br_{0.3}Cl_{0.1}$ active layer with different UVO treatment times after annealing are presented in Figure 10b. The PV characteristics of PSC are summarized in Table 2. The best-performing device observed in PSC in which the perovskite film was fabricated using 10 min of UVO-treated FAI/IPA solution. In this case, the best-performing PSC shows a PCE of 16.56% (J_{sc} = 22.97 mA/cm^2, V_{oc} = 1.07 V, and FF = 0.67) and 17.44% (J_{sc} = 23.08 mA/cm^2, V_{oc} = 1.07 V, and FF = 0.72) in forward and reverse sweep conditions, respectively.

Table 2. Device Parameters of $FAPbI_{2.6}Br_{0.3}Cl_{0.1}$ Films Fabricated by TSD Using UVO-Treated FAI Solution for Different Times

UV exposure time	scan direction	J_{sc} (mA/cm^2)	V_{oc} (V)	FF	PCE (%)
without	FS	18.16	1.08	0.57	11.1
	RS	18.46	1.08	0.67	13.39
1 min	FS	19.26	1.01	0.56	10.87
	RS	19.27	1	0.73	14.01
5 min	FS	22.63	1.07	0.65	15.66
	RS	22.43	1.07	0.72	17.29
10 min	FS	22.97	1.07	0.67	16.56
	RS	23.08	1.07	0.72	17.74
30 min	FS	21.09	1.07	0.55	12.31
	RS	20.89	1.06	0.72	16.05

The higher efficiency in the $FAPbI_{2.6}Br_{0.3}Cl_{0.1}$ active layer film is due to the well-organized, compact film fabricated by using an optimized UVO exposure time which produces FA^+ and I^- ions in the FAI/IPA solution. Most importantly, the perovskite films fabricated using UVO-treated FAI/IPA solution have better crystallinity compared to the perovskite films fabricated without UVO treatment.

Figure 10c shows the $J-V$ curves of the device characteristics of PSCs fabricated using UVO-treated FAI solution cast at different solution temperatures. The device characteristics are summarized in Table 3. The overall device performance

Table 3. Device Parameters of $FAPbI_{2.6}Br_{0.3}Cl_{0.1}$ Films Fabricated by TSD Using Hot-Casted UVO-Treated FAI Solutions

solution temperature	scan direction	J_{sc} (mA/cm^2)	V_{oc} (V)	FF	PCE (%)
80 °C	FS	19.45	1.06	0.67	13.8
	RS	20.14	1.07	0.74	16.05
100 °C	FS	20.44	1.07	0.66	14.46
	RS	20.42	1.07	0.75	16.34
120 °C	FS	23.22	1.09	0.66	16.78
	RS	23.4	1.09	0.75	19.22
140 °C	FS	16.89	1.13	0.65	12.52
	RS	17.24	1.11	0.74	14.19

significantly affected the hot-casting solution temperature. It is observed that the photovoltaic performance increases with FAI solution temperature up to 120 °C and decreases after 120 °C. From the results, it can be noted that the solar cell fabricated using hot FAI solution casting at 120 °C showed the best photovoltaic performances. In this case, the best-performing PSC shows a PCE of 16.76% (J_{sc} = 23.22 mA/cm^2, V_{oc} = 1.09 V, and FF = 0.66) and 19.22% (J_{sc} = 23.4 mA/cm^2, V_{oc} = 1.09 V, and FF = 0.75) in forward and reverse sweep conditions, respectively. This is related to the increase of α-$FAPbI_{2.6}Br_{0.3}Cl_{0.1}$ films and increases in grain size and crystallinity of the film.

CONCLUSIONS

In summary, we demonstrated a novel method of UVO treatment with FAI solutions to fabricate large grain α-$FAPbI_{2.6}Br_{0.3}Cl_{0.1}$ films. We observed just 10 min of UVO treatment to fabricate a compact, smooth, and pinhole-free α-$FAPbI_{2.6}Br_{0.3}Cl_{0.1}$ perovskite film. The dissociation of FAI into FA+ and I^- ions by UVO and thermal treatment of FAI

https://doi.org/10.1021/acsomega.2c07574
ACS Omega 2023, 8, 9298−9306

solutions enabled the diffusion of both ions into the PbI_2 octahedral space and reduce the iodine vacancy utilizing extra iodine atoms. In addition to that, the crystallinity of the perovskite films significantly increased with the UVO-treated FAI solution. We believe that the UVO-treated FAI solution provides an alternative method to fabricate the perovskite films and is quite a faster preparation method compared to the photoassisted and thermally assisted processes. The microstructure of the combined UVO and thermally assisted FAI solution shows an improved surface morphology in terms of compactness and grain size using UVO-treated FAI solution and optimized temperature of the hot-cast solution. With an optimized UVO-treated FAI solution and hot-casting at 120 °C, the PSCs showed the best PCE of 19.22%.

■ ASSOCIATED CONTENT

Supporting Information

The Supporting Information is available free of charge at https://pubs.acs.org/doi/10.1021/acsomega.2c07574.

UV−vis spectra of $FAPbI_{2.6}Br_{0.3}Cl_{0.1}$ films prepared by pure, UVO-treated and hot-cast of UVO-treated FAI solution; peak positions and FWHM of (001) peak of as-prepared (w/o and w/ annealing) perovskite films (PDF)

■ AUTHOR INFORMATION

Corresponding Authors

Bhabani Sankar Swain − *School of Materials Science and Engineering, Kookmin University, Sungbuk-gu, Seoul 136-702, Republic of Korea;* Present Address: Department of Chemical Engineering, Ajou University, Suwon, Gyeonggi-do 16499, Republic of Korea; orcid.org/0000-0003-1371-5657; Email: bsswain@kookmin.ac.kr, bsswain@ajou.ac.kr

Jaegab Lee − *School of Materials Science and Engineering, Kookmin University, Sungbuk-gu, Seoul 136-702, Republic of Korea*; Email: lgab@kookmin.ac.kr

Authors

Son Singh − *School of Materials Science and Engineering, Kookmin University, Sungbuk-gu, Seoul 136-702, Republic of Korea*

Rahim Abdur − *School of Materials Science and Engineering, Kookmin University, Sungbuk-gu, Seoul 136-702, Republic of Korea*

Jae-Hun Kim − *School of Materials Science and Engineering, Kookmin University, Sungbuk-gu, Seoul 136-702, Republic of Korea;* orcid.org/0000-0002-4252-2590

Complete contact information is available at: https://pubs.acs.org/10.1021/acsomega.2c07574

Notes

The authors declare no competing financial interest.

■ ACKNOWLEDGMENTS

This work was supported by the National Research Foundation of Korea (NRF) funded by the Ministry of Science and ICT (Grant Number: 2022R1A5A7000765).

■ REFERENCES

(1) Lee, J.-W.; Dai, Z.; Han, T.-H.; Choi, C.; Chang, S.-Y.; Lee, S.-J.; De Marco, N.; Zhao, H.; Sun, P.; Huang, Y.; et al. 2D Perovskite Stabilized Phase-Pure Formamidinium Perovskite Solar Cells. *Nat. Commun.* **2018**, *9*, 3021.

(2) Yun, J. S.; Ho-Baillie, A.; Huang, S.; Woo, S. H.; Heo, Y.; Seidel, J.; Huang, F.; Cheng, Y.-B.; Green, M. A. Benefit of Grain Boundaries in Organic-Inorganic Halide Planar Perovskite Solar Cells. *J. Phys. Chem. Lett.* **2015**, *6*, 875−880.

(3) Zhang, Y.; Li, Y.; Zhang, L.; Hu, H.; Tang, Z.; Xu, B.; Park, N.-G. Propylammonium Chloride Additive for Efficient and Stable $FAPbI_3$ Perovskite Solar Cells. *Adv. Energy Mater.* **2021**, *11*, 2102538.

(4) Hong, M. J.; Johnson, R. Y.; Labram, J. G. Impact of Moisture on Mobility in Methylammonium Lead Iodide and Formamidinium Lead Iodide. *J. of Phys. Chem. Lett.* **2020**, *11* (13), 4976−4983.

(5) Cheng, L.; Liu, Z.; Li, S.; Zhai, Y.; Wang, X.; Qiao, Z.; Xu, Q.; Meng, K.; Zhu, Z.; Chen, G. Highly Thermostable and Efficient Formamidinium-Based Low-Dimensional Perovskite Solar Cells. *Angew. Chem., Int. Ed.* **2021**, *60*, 856.

(6) Lv, S.; Pang, S.; Zhou, Y.; Padture, N. P.; Hu, H.; Wang, L.; Zhou, X.; Zhu, H.; Zhang, L.; Huang, C.; et al. One-step, Solution-Processed Formamidinium Lead Trihalide ($FAPbI_{(3-x)}Cl_x$) for Mesoscopic Perovskite-Polymer Solar Cells. *Phys. Chem. Chem. Phys.* **2014**, *16* (36), 19206−19211.

(7) Lee, D. G.; Kim, D. H.; Lee, J. M.; Kim, B. J.; Kim, J. Y.; Shin, S. S.; Jung, H. S. High Efficiency Perovskite Solar Cells Exceeding 22% via a Photo-Assisted Two-Step Sequential Deposition. *Adv. Funct. Mater.* **2021**, *31*, 2006718.

(8) Xu, F.; Tian, Y.; Wang, W.; Zhu, Y.; Zeng, L.; Yao, B.; Fang, Z.; Xu, H.; Xu, R.; Xu, F.; Hong, F.; Wang, L. In situ deposition of black α-$FAPbI_3$ films by vacuum flash evaporation for solar cells. *J. Mater. Sci. Mater. Electron.* **2019**, *30*, 8381−8389.

(9) Leyden, M. R.; Lee, M. V.; Raga, S. R.; Qi, Y. *J. Mater. Chem. A* **2015**, *3*, 16097−16103. Gu, L.; Zhang, D.; Kam, M.; Zhang, Q.; Poddar, S.; Fu, Y.; Mo, X.; Fan, Z. Significantly improved black phase stability of $FAPbI_3$ nanowires via spatially confined vapor phase growth in nanoporous templates. *Nanoscale* **2018**, *10*, 15164−15172.

(10) Lee, Y. M.; Yun, J.-H.; Matsuyama, A.; Kobori, S.; Maeng, I.; Lyu, M.; Wang, S.; Wang, L.; Jung, M.-C.; Nakamura, M. Significant THz-wave absorption property in mixed δ- and α-$FAPbI_3$ hybrid perovskite flexible thin film formed by sequential vacuum evaporation. *Appl. Phys. Express* **2019**, *12* (5), 051003.

(11) Borchert, J.; Milot, R. L.; Patel, J. B.; Davies, C. L.; Wright, A. D.; Martinez Maestro, L.; Snaith, H. J.; Herz, L. M.; Johnston, M. B. Large-area, highly uniform evaporated formamidinium lead triiodide thin films for solar cells. *ACS Energy Lett.* **2017**, *2*, 2799−2804.

(12) Xu, F.; Tian, Y.; Wang, W.; et al. In situ deposition of black α-$FAPbI_3$ films by vacuum flash evaporation for solar cells. *J. Mater. Sci: Mater. Electron* **2019**, *30*, 8381−8389.

(13) Zhang, Y. N.; Li, B.; Zhang, L. Y.; Yin, L. W. Efficient electron transfer layer based on Al_2O_3 passivated TiO_2 nanorod arrays for high performance evaporation-route deposited $FAPbI_3$ perovskite solar cells. *Sol. Energy Mater. Sol. Cells* **2017**, *170*, 187−196.

(14) Higgins, K.; Ziatdinov, M.; Kalinin, S. V.; Ahmadi, M. High-Throughput Study of Antisolvents on the Stability of Multicomponent Metal Halide Perovskites through Robotics-Based Synthesis and Machine Learning Approaches. *J. Am. Chem. Soc.* **2021**, *143* (47), 19945−19955.

(15) Meng, K.; Wang, X.; Xu, Q.; Li, Z.; Liu, Z.; Wu, L.; Hu, Y.; Liu, N.; Chen, G. In Situ Observation of Crystallization Dynamics and Grain Orientation in Sequential Deposition of Metal Halide Perovskites. *Adv. Funct. Mater.* **2019**, *29*, 1902319.

(16) Wang, Z.; Zhou, Y.; Pang, S.; Xiao, Z.; Zhang, J.; Chai, W.; Xu, H.; Liu, Z.; Padture, N. P.; Cui, G. Additive-Modulated Evolution of $HC(NH_2)_2PbI_3$ Black Polymorph for Mesoscopic Perovskite Solar Cells. *Chem. Mater.* **2015**, *27*, 7149−7155.

(17) Zhang, H.; Tu, C.; Xue, C.; Wu, J.; Cao, Y.; Zou, W.; Xu, W.; Wen, K.; Zhang, J.; Chen, Y.; Lai, J.; Zhu, L.; Pan, K.; Xu, L.; Wei, Y.; Lin, H.; Wang, N.; Huang, W.; Wang, J. Low Roll-Off and High Stable Electroluminescence in Three-Dimensional $FAPbI_3$ Perovskites with Bifunctional-Molecule Additives. *Nano Lett.* **2021**, *21* (9), 3738−3744.

https://doi.org/10.1021/acsomega.2c07574
ACS Omega 2023, 8, 9298−9306

(18) Shin, G. S.; Zhang, Y.; Park, N.-G. Stability of Precursor Solution for Perovskite Solar Cell: Mixture (FAI + PbI_2) versus Synthetic $FAPbI_3$ Crystal. *ACS Appl. Mater. Interfaces* **2020**, *12* (13), 15167−15174.
(19) Akin, S.; Akman, E.; Sonmezoglu, S. $FAPbI_3$-Based Perovskite Solar Cells Employing Hexyl-Based Ionic Liquid with an Efficiency Over 20% and Excellent Long-Term Stability. *Adv. Funct. Mater.* **2020**, *30*, 2002964.
(20) Lu, H.; Liu, Y.; Ahlawat, P.; Mishra, A.; Tress, W. R.; Eickemeyer, F. T.; Yang, Y.; Fu, F.; Wang, Z.; Avalos, C. E.; Carlsen, B. I.; Agarwalla, A.; Zhang, X.; Li, X.; Zhan, Y.; Zakeeruddin, S. M.; Emsley, L.; Rothlisberger, U.; Zheng, L.; Hagfeldt, A.; Grätzel, M. Vapor-assisted deposition of highly efficient, stable black-phase $FAPbI_3$ perovskite solar cells. *Science* **2020**, *370*, No. eabb8985.
(21) Jeong, J.; Kim, M.; Seo, J.; et al. Pseudo-halide anion engineering for α-$FAPbI_3$ perovskite solar cells. *Nature* **2021**, *592*, 381−385.
(22) Eperon, G. E.; Stranks, S. D.; Menelaou, C.; Johnston, M. B.; Herz, L. M.; Snaith, H. J. Formamidinium lead Trihalide: a Broadly Tunable Perovskite for Efficient Planar Heterojunction Solar Cells. *Energy Environ. Sci.* **2014**, *7*, 982−988.
(23) Park, B.; Kwon, H. W.; Lee, Y.; et al. Stabilization of formamidinium lead triiodide α-phase with isopropylammonium chloride for perovskite solar cells. *Nat. Energy* **2021**, *6*, 419−428.
(24) Leyden, M. R.; Lee, M. V.; Raga, S. R.; Qi, Y. Large formamidinium lead trihalide perovskite solar cells using chemical vapor deposition with high reproducibility and tunable chlorine concentrations. *J. Mater. Chem. A* **2015**, *3*, 16097−16103.
(25) Lyu, M.; Lee, D. K.; Park, N.-G. Effect of alkaline earth metal chloride additives BCl_2 (B = Mg, Ca, Sr, and Ba) on the photovoltaic performance of $FAPbI_3$ based perovskite solar cells. *Nanoscale Horiz.* **2020**, *5*, 1332−1343.
(26) Yao, D.; Zhang, C.; Pham, N. D.; Zhang, Y.; Tiong, V. T.; Du, A.; Shen, Q.; Wilson, G. J.; Wang, H. Hindered formation of photoinactive δ-$FAPbI_3$ phase and hysteresis-free mixed-cation planar heterojunction perovskite solar cells with enhanced efficiency via potassium incorporation. *J. Phys. Chem. Lett.* **2018**, *9*, 2113−2120.
(27) Hu, Y.; Qiu, T.; Bai, F.; Miao, X.; Zhang, S. Enhancing moisture-tolerance and photovoltaic performances of $FAPbI_3$ by bismuth incorporation. *J. Mater. Chem. A* **2017**, *5* (48), 25258−25265.
(28) Zhang, Y.; Seo, S.; Lim, S. Y.; Kim, Y.; Kim, S.-G.; Lee, D.-K.; Lee, S.-H.; Shin, H.; Cheong, H.; Park, N.-G. Achieving Reproducible and High-Efficiency (>21%) Perovskite Solar Cells with a Presynthesized $FAPbI_3$ Powder. *ACS Energy Lett.* **2020**, *5* (2), 360−366.
(29) Deng, W.; Li, F.; Li, J.; Wang, M.; Hu, Y.; Liu, M. Anti-solvent free fabrication of FA-Based perovskite at low temperature towards to high performance flexible perovskite solar cells. *Nano Energy* **2020**, *70*, 104505.
(30) He, W.; Hu, J.; Chen, C.; Chen, Y.; Zeng, L.; Zhang, X.; Cai, B.; Mai, Y.; Guo, F. Temperature-assisted crystal growth of photovoltaic alpha-phase $FAPbI_3$ thin films by sequential blade coating. *ACS Appl. Mater. Interfaces* **2020**, *12*, 55830−55837.
(31) Baltakesmez, A. $FAPbI_3$ perovskite thin film having α/δ phase junction and its light-harvesting performance in solar cell. *J. Mater. Sci: Mater. Electron* **2020**, *31*, 17773−17783.

https://doi.org/10.1021/acsomega.2c07574
ACS Omega 2023, 8, 9298−9306